Journal Pre-proof

Interplay between potato virus X and RNA granules in *Nicotiana benthamiana*

Robles-Luna Gabriel, Furman, Nicolás, Barbarich María Florencia, Carlotto Nicolás, Attorresi Alejandra, García, María Laura, Kobayashi Ken

PII: S0168-1702(19)30618-5

DOI: https://doi.org/10.1016/j.virusres.2019.197823

Reference: VIRUS 197823

To appear in: *Virus Research*

Received Date: 23 August 2019

Revised Date: 16 November 2019

Accepted Date: 20 November 2019

Please cite this article as: Robles-Luna G, Furman, N, Barbarich MF, Carlotto N, Alejandra A, García, ML, Kobayashi K, Interplay between potato virus X and RNA granules in *Nicotiana benthamiana*, *Virus Research* (2019), doi: https://doi.org/10.1016/j.virusres.2019.197823

Interplay between potato virus X and RNA granules in *Nicotiana benthamiana*

RUNNING TITLE: PVX effects on RNA granules

Robles-Luna, Gabriel[1]; Furman, Nicolás[2#1]; Barbarich, María Florencia[2#2]; Carlotto, Nicolás[2], Attorresi, Alejandra[3]; García, María Laura[1] and Kobayashi, Ken[2]*

1. Instituto de Biotecnología y Biología Molecular (IBBM)-CONICET-UNLP, Calle 115 y 49 s/n (1900), Universidad Nacional de la Plata, Facultad de Ciencias Exactas, La Plata, Argentina.

2. Instituto de Biodiversidad y Biología Experimental y Aplicada (IBBEA, CONICET-UBA), Laboratorio de Agrobiotecnología, Facultad de Ciencias Exactas y Naturales, Departamento de Fisiología, Biología Molecular y Celular (FBMC), Universidad de Buenos Aires, Buenos Aires, Argentina.

3. Instituto de Investigación en Biomedicina de Buenos Aires (IBioBA) -CONICET- Partner Institute of the Max Planck Society.

[#1]. Present address: Banco Nacional de Datos Genéticos, Buenos Aires, Argentina.

[#2]. Present address: Universidad de Buenos Aires, Facultad de Filosofía y Letras, Instituto interdisciplinario de Tilcara, Argentina.

* Corresponding author: ken@fbmc.fcen.uba.ar; Phone:+54 011 52858406.

Emails: Robles-Luna Gabriel:garobles@gmail.com; Nicolás Furman: nicofurman@gmail.com, María Florencia Barbarich: fbarbarich@fbmc.fcen.uba.ar, Nicolás Carlotto:

carlotto.nicolas@gmail.com, Alejandra Attorresi: aleatto@gmail.com, María Laura García: garcia_m@biol.unlp.edu.ar.

Highlights

- Plant stress granule (SG) is not induced by potato virus X (PVX) infection.
- PVX inhibits SG assembly induced by hypoxia
- PVX induced X-body associates with AtUBP1b (SG component)
- Co-expression of AtUBP1b may inhibit the onset of PVX infection.

ABSTRACT

Cytoplasmic RNA granules consist of microscopic agglomerates of mRNAs and proteins and occur when the translation is reversibly and temporally halted (stress granules, SGs) or mRNAs are targeted for decapping (processing bodies, PBs). The induction of RNA granules formation by virus infection is a common feature of mammalian cells. However, plant-virus systems still remain poorly characterized. In this work, the SG marker AtUBP1b was expressed in *Nicotiana benthamiana* plants to decipher how the virus infection of plant cells affects SG dynamics. We found that the hypoxia-induced SG assembly was substantially inhibited in Potato virus X (PVX)-infected cells. Furthermore, we determined that the expression of PVX movement protein TGBp1 by itself, mimics the inhibitory effect of PVX on SG formation under hypoxia. Importantly, overexpression of AtUBP1b showed inhibition of the PVX spreading, whereas the overexpression of the dominant negative AtUBP1brrm enhanced PVX spreding, indicating that AtUBP1b negatively affects PVX infection. Notably, PVX infection did not inhibit the formation of processing bodies (PBs), indicating

PVX has distinct effects depending on the type of RNA granule. Our results suggest that SG inhibition could be part of the virus strategy to infect the plant.

KEYWORDS: PVX, SGs, X-body, AtUBPb1, PBs, DCP1.

1. INTRODUCTION

Cellular stress responses involve diverse intra- and extracellular signals that generally provokes mRNAs translational arrest with subsequent formation of cytoplasmic RNA granules (Sorenson and Bailey-Serres, 2014; Weber et al., 2008; Chantarachot and Bailey-Serres, 2017). These cytoplasmic granules are conserved in animals and plants, and their assembly is fast and reversible (when the stimulus dissipates), constituting a very dynamic post-transcriptional regulatory mechanism of gene expression (Kedersha et al., 2005). RNA granules can be classified according to their specific components and functions (Anderson & Kedersha, 2006).

Stress granules (SG) are ribonucleic protein complex containing stalled translation initiation complexes, initiation factors, small subunit of ribosome, and mRNA (Anderson and Kedersha, 2009; Panas et al., 2016), where a temporal pause of mRNA translation occurs. SG formation can be induced artificially by external stresses such as UV radiation/light, oxidative stress, peroxide, hypoxia, or heat (Anderson and Kedersha, 2009, 2006). In plants, two nuclear proteins called oligouridylate-binding protein 1b (UBP1b) and RNA-binding protein 47b (RBP47b) are assigned as plant SG markers (Weber et al., 2008) and are both orthologous to TIA-1 and TIA-1-like proteins of mammalian cells (Lambermon et al., 2000; Lorkovic et al., 2000). These proteins contain a prion-like domain at their amino terminal end, and three RNA recognition domains arranged in tandem (Weber et al., 2008). Another cytoplasmic RNA granule found in plants is the processing body (PB) where the mRNA decapping occurs. The PB is composed mainly of

decapping protein 1 (DCP1), DCP2, DCP5, and Varicose (Weber et al., 2008, Xu *et al.*, 2006). In contrast to SGs, the presence of PBs in the cytoplasm is constitutive, although their number can vary upon different stimulus, as reported in plant protoplasts (Weber et al., 2008), revealing their critical role in cytoplasmic RNA homeostasis (Xu *et al.*, 2006).

Viruses are obligatory intracellular parasites and completely depend on host translational machinery to produce viral proteins. Considering that SGs play a critical role in cellular translation regulation, it was proposed that virus infections in eukaryotic cells may affect SG dynamics and vice-versa. Indeed, it was shown that SG formation is induced during mammalian virus infections, which has been associated with an antiviral effect (Beckham and Parker, 2008; Lloyd, 2012). There are also reports describing some mammalian viruses that have evolved strategies to overcome the cellular stress response (Valiente-Echeverría et al., 2012; Beckham and Parker, 2008; Montero and Trujillo-Alonso, 2011; White and Lloyd, 2012). For instance, the poliovirus genome encodes a protease 3CPro protein that cleaves G3BP-1, a critical component for SG formation (White et al., 2007). Also, West Nile virus and dengue virus recruit the SG proteins TIA-1/R into virus replication sites (Emara and Brinton, 2007), hinting about a mechanism to mitigate the cell stress response, although its potential effect on infection was not evaluated. Similarly, animal viruses are also capable to modulate the formation of PBs in host cells, that would allow continuing the use of critical host factors for own replication (Beckham & Parker, 2008, Montero & Trujillo-Alonso, 2011, White & Lloyd, 2012). In contrast, there are only few studies reporting the interaction between plant virus and RNA granules (Conti et al., 2017; Hafrén et al., 2015; Krapp et al., 2017). For example, a conserved plant SG component was shown to interact with the nuclear shuttle protein from nanovirus pea necrotic yellow dwarf virus and geminivirus abutilon mosaic virus (Krapp et al., 2017; Mäkinen et al., 2017).

Potato virus X (PVX) is the type member of the genus potexvirus and has a monopartite genome composed of a single, positive strand 6.4 kb genomic RNA (gRNA) encoding five open reading

frames (ORFs). The replication of PVX consists in the synthesis of both strands of gRNA and subgenomic RNAs (Price, 1992), and the positive-strand RNAs have a 5´ Cap (Sonenberg et al., 1978) and a 3' poly-A tail (Price, 1993). In *Nicotiana benthamiana*, PVX produces local and systemic infection and the typical symptoms are concentric chlorosis, vascular clearing or mottled chlorosis.

There is a generally accepted idea that viruses could have co-evolved counter-defense mechanisms to overcome the adverse cellular context provoked by the cell stress response mediated by RNA granules (Valiente-Echeverria *et al.*, 2012). However, this remains unexplored in plants under virus infection. Here, we evaluated the interplay between PVX and RNA granules assembly.

2. MATERIALS AND METHODS

2.1. DNA constructs

The cDNA of GFP:AtUBP1b was subcloned from the plasmid pRTdS GFP kindly obtained from Dr. Fauth (Goethe-Universität Frankfurt, Germany) into the destination vector pK7WG2DΔGFP, kindly provided by Dr. Zelada (IBBEA, CONICET-UBA, Argentina). Similarly, RFP:RBP47b (At1g19130) was from Dr. Fauth (Goethe-Universität Frankfurt, Germany). AtUBP1b coding sequence was also subcloned into the vector pK7RWG2, kindly provided by the Department of Plant Systems Biology at the VIB-Ghent University, to produce RFP:AtUBP1b fusion. PVX-GFP infective clone and TGBp1:mCherry was kindly provided by Dr. MacFarlane and Dr. Tilsner (The James Hutton Institute, Dundee, Scotland UK). The AtUBP1b mutant (His:AtUBP1brrm) constructs was kindly provided by Dr. Mäkinen (Hafrén et al., 2015) and Dr. Fauth. The PB´s marker AtDCP1:RFP fusion was kindly obtained from Dr. Gagliardi (Sement et al., 2013). RFPer was kindly provided by Dr. Nelson (Nelson et al., 2007).

2.2. Plant growth conditions and agroinfiltration

Nicotiana benthamiana plants were grown in a growth chamber with 16 h daylight and 8 h of dark at a constant temperature (24°C) for 4-6 weeks. Transient expression in *N. benthamiana* was performed by agroinfiltration. At 48 h post-agroinfiltration, leaf disks were excised and observed by confocal or epifluorescence microscopy. Hypoxia treatment consisted of vacuum infiltration with distilled water and then sealed with synthetic enamel. Cicloheximide treatment (100 µg/ml) was performed according to Weber et al., 2008.

2.3. PVX inoculation

PVX inoculum obtained from PVX-infected leaf sap resuspended in phosphate buffer 0.1 M was applied directly on top of the leaf and inoculated mechanically by soft rubbing. Alternatively, *Agrobacterium* cultures carrying the PVX-GFP or PVX infectious clones were infiltrated into the abaxial side of leaves. For the early phase infection experiment, *Agrobacterium* cultures carrying the PVX clone at the optical density (OD_{600nm})= 0.2 was agroinfiltrated, a condition that all cells became evenly infected. For RNA granules counting, the 5 days post-infected (dpi) leaves were infiltrated with *Agrobacterium* cultures carrying SG or PB marker. Also, *Agrobacterium* cultures of PVX-GFP ($OD_{600nm} = 10^{-5}$) and mRFP, RFP:AtUBP1b, His:AtUBP1brrm, or AtDCP1:RFP ($OD_{600nm} = 0.1$), were infiltrated in the abaxial side of the leaf.

2.4. Confocal microscopy

CLSM was performed using Leica SP5 confocal microscope with a HCX PL APO CS 63.0x1.4 Oil UV objective lens in sequential mode using the LAS AF version 211 2.2.1 4842 software. Images stacks were processed with Image J software. Alternatively, images were acquired with an LSM 710 Axio Observer inverted microscope (ZEISS). Data acquisition was controlled by Zen Blue 2011 software (ZEISS) and the images were processed with Zen Black 2011 software (ZEISS). Cells were imaged with a 40X water objective (Plan-Apochromat 1.20W M27).

2.5. Western blot

Leaf protein extracts were analyzed in SDS–polyacrylamide gel electrophoresis (PAGE) and transferred to nitrocellulose membrane (Amersham™ Hybond ECL). GFP protein was detected with an anti-GFP polyclonal antibody (ab290; Abcam Ltd Cambridge, UK). Alkaline phosphatase-conjugated goat anti-rabbit antibody (BioRad, CA, USA) followed by BCIP/NBT detection. Band intensities of GFP were quantified using Image J software normalizing to RFP control bands from the half leaf of each plant. The band intensities were also normalized with the bands of ribulose 1, 5- bisphosphate carboxylase/oxygenase large subunit (rbcl, 55kDa – Ponceau staining) to estimate total protein loads.

2.6. Statistical analyses.

For quantitative analyses, SGs and PBs were eye counted on the maximum projection of each stack and expressed as a number of granules/cell. Infected or uninfected cells expressing the markers were used for counting manually from at least two independent experiments (Supplemental Table S1). Box & Whiskers with 90-10 percentiles were plotted for each treatment and ANOVA analysis was performed. Calculations were done with the GraphPad Prism version 5.00 software (p-value = 0.0001). SS = sum of squares; df = degrees of freedom; MS = mean square. Also, multiple comparison analyses of SG formation frequencies between different treatments were performed by a Tukey's Multiple Comparison Test, using the data shown in Supplemental Table S1. For halo measurements, an analysis was performed using the Kruskal–Wallis followed with Dunn's contrasts method (Supplemental table S5) with the data shown in Supplemental table S4.

2.7. qRT-PCR

SYBR® Green was used for PCR mixes. All reactions were run in triplicate for each sample at CFX96 Touch Real-Time PCR Detection system (Bio-Rad, Hercules, CA, USA). The primers for

gPVX correspond to CP ORF. Values were relativized to that for actin or PP2A Protein phosphatase 2A (At1g13320). Averages of three independent reactions ± standard deviations (s.d) were determined. The relative expression level was calculated using the $2^{-\Delta CT}$ and fold determined by using $2^{-\Delta\Delta CT}$ method.

3. RESULTS

3.1. Dynamic SG formation in *N. benthamiana* cells under hypoxia stress

The *Arabidopsis* UBP1b (AtUBP1b) is considered a plant SG marker (Weber et al., 2008) and GFP:AtUBP1b translational fusion expression in *N. benthamiana* cells revealed a strong signal mainly in the nucleus and to a lesser extent in the cytoplasm (Fig. S1Ai). Thirty minutes of hypoxia condition was enough to induce granule-like structures in the cytoplasm, showing an increase in size, number, and motility over time. This time-frame was similar with those reported for SGs in protoplasts (Weber et al., 2008) or AtUBP1c fusion protein in plants under hypoxia (Sorenson and Bailey-Serres, 2014). Similar results were observed with another SG marker RFP:RBP47b (Fig. S1B). To further confirm the identity of these dynamic granules as SGs under hypoxia, the GFP:AtUBP1b expressing leaves were pre-treated with cycloheximide, which significantly inhibited the formation of SGs in the cytoplasm, as previously reported (Weber et al., 2008) (Fig. S1Aii).

3.2. PVX infection of *N. benthamiana* triggers re-localization of SGs marker into larger aggregates

Animal virus-induced SGs are often dynamic and they may be present for a short period at some specific stage of infection. To evaluate whether PVX induces SG assembly, a time-course of SG formation was monitored during an earlier phase of PVX infection. To this end, GFP:AtUBP1b was expressed at 24 h previous to PVX inoculation and the SG formation checked by microscopy at 7, 12, 18, 24 and 48 hours (h) post-inoculation. As shown in the Fig. 1A, only very few SGs

were observed, even at 24 and 48 h when virus multiplication is higher (Fig. 1B). When the non-infected control was evaluated and compared, no significant difference in the SGs formation was observed (data not shown), indicating that SGs are not induced during early stages of PVX infection.

We also studied the SG dynamics when PVX infection was established. For this, PVX was first inoculated onto *N. benthamiana* leaf either by mechanical inoculation with sap from a fully infected leaf or agroinfiltration of infective PVX clone, allowing full local infection at 5 days post-inoculation (dpi). A day before, at 4 dpi, RFP:AtUBP1b was expressed on the infected leaf by agroinfiltration. As shown in Fig 2Aiii, PVX did not induce the SG formation at 5 dpi, similarly to the earlier infection stages. However, few large aggregates/clusters labeled with RFP:AtUBP1b were consistently observed in infected cells. These large aggregates were distinct in frequency, sizes, and shapes among them, and differ from those observed under stress (Sorenson et al. 2014), and therefore were not considered as SGs. Similar results were observed using RBP47b as a SG marker (Fig. S1B). Therefore, we conclude that PVX infection does not induce SG formation, but rather re-localizes SGs proteins into large aggregates.

3.3. PVX infection affects negatively SG formation

In view that PVX did not induce the SG formation, we applied hypoxia stress on AtUBP1b expressing leaves, and observed the effect of the PVX infection on the SG formation. Firstly, in uninfected cells, upon hypoxia stress, RFP:AtUBP1b was observed in the nucleus (N), cytoplasm and located into SGs (Fig. 2Aii upper row, Fig. S1). These SGs were highly mobile as depicted in the color-frame stack on Fig. 2Aii lower row (see also Supplemental videos). In response to PVX infection, RFP:AtUBP1b located in the nucleus, cytoplasm and immobile large aggregates often in proximity to the nucleus (Fig. 2Aiii). Furthermore, immobile fewer SGs were also visualized with hypoxia (Fig. 2Aiv and 2B, supplemental video S8). These results indicated that PVX inhibits SG

formation normally induced by abiotic stress and reduces intracellular motility of the few small SGs.

3.4. AtUBP1 is recruited into PVX X-bodies

Regarding the large aggregates of RFP:AtUBP1 observed in PVX-infected cells (Fig. 2Aiii, iv), we wondered if these clusters would resemble those cytoplasmic inclusion bodies induced by plant virus, called X-body for PVX, associated with the viral replication complex of infected cells (Cruz et al., 1998; Davies et al., 1993; Kozar and Sheludko, 1969; Stols et al., 1970; Tilsner et al., 2012). It was previously reported that PVX encoded TGBp1 is responsible for the cytoskeleton and ER rearrangement into the formation of X-body, which contains the rest of PVX proteins and viral RNAs (vRNAs). Notably, TGBp1 expression alone is also able to build a similar inclusion body, called pseudo-X-body, consisting of a large aggregate of TGBp1, actin, and ER (Tilsner et al., 2012).

To evaluate whether the observed inhibition of SGs and the formation of large clusters of AtUBP1b in infected cells were linked to the presence of virus-induced inclusion bodies, we assessed the effect of TGBp1:mCherry co-expression during SGs formation under the same conditions. We found clusters of SG-like granules and GFP:AtUBP1b aggregates very close toTGBp1:mCherry labelled inclusion bodies (Fig. 3A). Furthermore, the GFP:AtUBP1b cluster was also observed next to the X-body in infected cells revealed by TGBp1:mCherry (Fig. 3B) or ER maker RFPer (Fig. S2). These results were unexpected since none of the X-body (or pseudo X-body) components, such as ER, were previously reported to interact with SGs nor AtUBP1b, and suggest that the SG component AtUBP1b is recruited into the proximity of PVX viral replication complex (or inclusion body) indirectly.

The presence of inclusion body not only affected AtUBP1b subcellular localization but also lowered the frequency of SGs compared to cells expressing GFP:AtUBP1b alone in the same

condition, showing the similar inhibitory effect observed in PVX infected cells, although to a lesser extent (Fig. 2B). These results further support that PVX has an impact on the dynamics of SGs, and this is probably mediated by endomembrane and cytoskeleton alterations during the assembly of inclusion body.

3.5. AtUBP1b affects PVX infection

To further investigate the interplay between PVX and SGs, we evaluated the potential effects of AtUBP1b over-expression during the onset of PVX infection. For this, RFP:AtUBP1b expressing *Agrobacterium* was infiltrated on the half leaf (OD_{600nm}=0.1). As a control, instead RFP:AtUBP1b, free mRFP (monomeric red fluorescent protein) was also infiltrated on the other half of the same leaf. After 24 h, a diluted culture ($OD_{600nm} = 10^{-5}$) of *Agrobacterium* carrying PVX-GFP viral vector was infiltrated on the same leaf to obtain isolated GFP spots in order to visualize the spread of the PVX-infection, later by measuring the size of GFP fluorescent foci at 5 dpi. As shown in Figure 4, the area of infection foci in RFP:AtUBP1-infected half leaf was significantly smaller compared to the corresponding half leaf expressing the control mRFP.

To determine whether the size reduction of the GFP foci was a consequence of decreased virus replication in the presence of AtUBP1b, vRNAs accumulation was titered using RT-qPCR in parallel samples. In RFP:AtUBP1b infiltrated half leaves, no significant difference of vRNA accumulation was found compared to mRFP controls (Fig. 4C and S6), although GFP protein level estimated by immunoblot showed a reduced GFP accumulation in RFP:AtUBP1b half leaves compared with mRFP controls (Fig. 4D).

To further confirm the negative effect of AtUBP1b during PVX infection, we assessed the impact of a dominant negative mutant version of AtUBP1b protein expression, AtUBP1brrm, which can supress the action of the endogenous pool of UBP1b and the formation of basal SGs (Weber et al., 2008, Hafrén et al., 2015). We found a significant larger size of PVX-GFP spots in

AtUBP1brrm-expressing leaves than those expressing the controls mRFP or AtUBP1b (Fig 4A and B). Accordingly, higher accumulation of GFP was determined in AtUBP1brrm-expressing leaves compared with mRFP controls or AtUBP1b expressing leaves (Fig. 4D). Notably, the vRNAs levels in AtUBP1brrm-expressing leaves also showed a slight increase compared with mRFP, but significantly higher compared to RFP:AtUBP1b infiltrated leaves (Fig. 4C and S6). These results indicated that SGs have an impact during the onset of the PVX infection, likely involving the UBP1 protein.

3.6. PVX infection induces PBs formation

In view of our results with SG, we wondered if PVX could also affect the PB formation. For this purpose, we used AtDCP1:RFP fusion protein as PB marker in transient expression in healthy and PVX-GFP-infected *N. benthamiana* plants. First, we observed the constitutive presence of 30 to 250 PBs per cell when AtDCP1:RFP fusion protein was expressed (Fig. 5Ai). In PVX-GFP infected cells, a small but significant increment of the PB frequencies was consistently observed (Fig. 5B). In contrast to SGs, the intracellular motility of PBs was not affected in infected cells (Fig. S4 and supplemental video S4).

Since the abiotic stress could affect the response against the virus, we also repeated the experiment under hypoxia. As shown in Fig. 5B and Fig. S4, no changes in PB frequency was observed, indicating PBs formation does not respond to hypoxia treatment. Similarly, we evaluated if PVX infection is inhibited by AtDCP1 over-expression. Contrary to the effects observed with AtUBP1b and AtUBP1brrm overexpression, no significant differences in the foci size between the half leaf expressing free mRFP controls and AtDCP1:RFP were observed (Fig. 5C). Altogether, our results indicate that PVX induces the PB formation, but AtDCP1 overexpression has no effect on PVX spreading.

4. DISCUSSION

Here we investigated the effect of PVX on the formation of RNA granules in *N. benthamiana*. We determined that PVX infection does not induce the formation of SGs. In addition, we found that the formation of SGs was inhibited in infected cells and the SG component AtUBP1b levels had an impact during the establishment of PVX-GFP infection. Moreover, we found an intriguing reduced movement of a few remaining SGs in PVX infected cells, together with the presence of large structures labelled with RFP:AtUBP1b. Microscopy images revealed that those large structures were closely associated with viral-induced X-bodies.

To explain this phenomenon, we reasoned that during the formation of the X-body in which the intracellular disorganization of cytoskeleton and ER takes place, it might also alter the intracellular movement of SGs, inhibiting their assembly. That is the case in animal cells, in which the pharmacological activation of 5'-AMP-activated protein kinase involved during stress sensing, produces a loss of histone deacetylase 6 accompanied by increased acetylation of α-tubulin, which in turns induce SGs but inhibiting the formation of larger SGs (Mahboubi et al., 2016). Consequently, the change in microtubule could limit SGs movement and fusion into larger granules. In addition, ER integrity would be also critical for SGs assembly, as suggested by a fewer SGs formation observed in animal cell with a reduced level of the TRAnsport Protein Particle (TRAPP) complex, which controls ER-to-Golgi trafficking during the secretory pathway (Zappa et al., 2019). In agreement, the pseudo-X-body formation that modifies endomembrane and cytoskeleton organization also reduces SG formation by inducing large RFP:AtUBP1b clusters at the pseudo-X-body.

The SGs motility was previously described to be mainly dependent on microtubules (Bartoli et al., 2011; Ivanov et al., 2003). A preliminary experiment using TUA:GFP expressing transgenic *N. benthamiana* infecting with PVX showed, likewise in healthy plants, cells with the microtubule

fishnet-like structure labeled with TUA:GFP. However, intense TUA:GFP regions were consistently visible at the periphery of the infected cells (Supplemental Figure S5). Altogether, we propose PVX mediated modification of the cellular cytoskeleton as a potential SGs assembly inhibition mechanism that affects SGs motility in infected cells.

To further support the interplay between SGs and PVX, we also found that the overexpression of AtUBP1b reduces the expression of GFP from PVX-GFP (determined by measuring the GFP foci and protein level) accompanying with a slight decrease in the accumulation of vRNAs. This suggests that an increased level of AtUBP1b has a negative effect during virus replication and/or translation. Indeed, the PVX-GFP spreading was enhanced (with increased accumulation of GFP) by expressing a dominant negative mutant AtUBP1brrm, which impairs the action of endogenous UBP1b protein, supporting again that SGs level has an effect during PVX infection. Therefore, we propose a model in which the excess of AtUBP1b through its RNA binding domains would inhibit vRNAs translation and alternatively, AtUBP1brrm would prevent the interaction of endogenous UBP1 with vRNAs and consequently enhance the virus translation. Nevertheless, further experiments will be required to determine the mechanisms involved during the interplay between PVX and SGs.

In a previous report, Ma et al., (2015) linked the accumulation of capped vRNAs with the increasing aggregation of PBs during the plant recovery from TRV infection. The PVX genome and its sub-genomic RNAs contain 5´Cap, therefore we can speculate that the observed PB formation is the result of the accumulation of these capped vRNAs, as a defense mechanism.

In summary, PVX affects differentially cytoplasmic RNA granules formation and dynamics, which can be associated with the virus mechanism to achieve a successful infection.

5. CONCLUSION

Our results hint at an interplay between PVX and cytoplasmic RNA granules dynamics. We propose that PVX would have evolved a SG formation inhibitory mechanism to counteract the plant stress response to allow an efficient infection, similar to what has been described for the animal virus. Our results give an insight into a potential virus adaptation to plant stress response.

Author Statement

Here we resubmit the revised version of our manuscript entitled ***"Interplay between potato virus X and RNA granules in Nicotiana benthamiana***" by Robles-Luna et al. We have performed additional experiments and address all comments of each of the reviewers in detail**.** Please, find all changes incorporated in the manuscript highlighted in yellow as requested.

Acknowledgment:

This work was initially funded by University of Buenos Aires (UBACyT, 20020090200172). GRL, MFB and NC were supported by Research Fellowships from the National Research Council (CONICET). NF was supported by ANPCyT. AA, MLG, and KK belong to CONICET. This work was partially supported by CONICET and ANPCyT from Argentina. We thank Eduardo Peña, Jens Tilsner, Carolina Perez Castro, and Federico Ariel for helpful discussion and critical reading of the manuscript. We want to thank the confocal microscopy facilities and technicians (Plataforma de Microscopía avanzada, UNLP).

References

Anderson, P., Kedersha, N., 2009. Stress granules. Curr. Biol.19,R397-8. https://doi.org/10.1016/j.cub.2009.03.013

Anderson, P., Kedersha, N., 2006. RNA granules. J. Cell Biol. 172, 803–808. https://doi.org/10.1083/jcb.200512082

Bartoli, K.M., Bishop, D.L., Saunders, W.S., 2011. The role of molecular microtubule motors and the microtubule cytoskeleton in stress granule dynamics. Int. J. Cell Biol. 2011, 1–10.

https://doi.org/10.1155/2011/939848

Beckham, C.J., Parker, R., 2008. Review P Bodies , Stress Granules , and Viral Life Cycles. https://doi.org/10.1016/j.chom.2008.03.004

Conti, G., Zavallo, D., Venturuzzi, A.L., Rodriguez, M.C., Crespi, M., Asurmendi, S., 2017. TMV induces RNA decay pathways to modulate gene silencing and disease symptoms. Plant J. 89, 73–84. https://doi.org/10.1111/tpj.13323

Cruz, S.S., Roberts, A.G., Prior, D.A.M., Chapman, S., Oparka, K.J., 1998. Cell-to-Cell and Phloem-Mediated Transport of Potato Virus X: The Role of Virions, The Plant Cell 10, 495-510. https://doi.org/10.1105/tpc.10.4.495

Davies, C., Hills, G., Baulcombe, D.C., 1993. Sub-cellular Localization of the 25-kDa Protein Encoded in the Triple Gene Block of Potato Virus X. Virology 197, 166–175. https://doi.org/10.1006/VIRO.1993.1577

Emara, M.M., Brinton, M.A., 2007. Interaction of TIA-1/TIAR with West Nile and dengue virus products in infected cells interferes with stress granule formation and processing body assembly. Proc. Natl. Acad. Sci. 104, 9041–9046. https://doi.org/10.1073/pnas.0703348104

Hafrén, A., Lõhmus, A., Mäkinen, K., 2015. Formation of Potato Virus A-Induced RNA Granules and Viral Translation Are Interrelated Processes Required for Optimal Virus Accumulation. PLoS Pathog. 11, 1–28. https://doi.org/10.1371/journal.ppat.1005314

mmanuel, T.M., Greenwood, D.R., MacDiarmid, R.M., 2012. A critical review of translation initiation factor eIF2?? kinases in plants - Regulating protein synthesis during stress. Funct. Plant Biol. 39, 717–735. https://doi.org/10.1071/FP12116

Ivanov, P.A., Chudinova, E.M., Nadezhdina, E.S., 2003. Disruption of microtubules inhibits cytoplasmic ribonucleoprotein stress granule formation. Exp. Cell Res. 290, 227–233. https://doi.org/10.1016/S0014-4827(03)00290-8

Kedersha, N., Stoecklin, G., Ayodele, M., Yacono, P., Lykke-Andersen, J., Fitzler, M.J.,

Scheuner, D., Kaufman, R.J., Golan, D.E., Anderson, P., 2005. Stress granules and processing bodies are dynamically linked sites of mRNP remodeling. J. Cell Biol. 169, 871–884. https://doi.org/10.1083/jcb.200502088

Kozar, F.E., Sheludko, Y.M., 1969. Ultrastructure of potato and Datura stramonium plant cells infected with potato virus X. Virology 38, 220–229. https://doi.org/10.1016/0042-6822(69)90363-8

Krapp, S., Greiner, E., Amin, B., Sonnewald, U., Krenz, B., 2017. The stress granule component G3BP is a novel interaction partner for the nuclear shuttle proteins of the nanovirus pea necrotic yellow dwarf virus and geminivirus abutilon mosaic virus. Virus Res. 227, 6–14. https://doi.org/10.1016/j.virusres.2016.09.021

Lambermon, M.H., Simpson, G.G., Wieczorek Kirk, D.A., Hemmings-Mieszczak, M., Klahre, U., Filipowicz, W., 2000. UBP1, a novel hnRNP-like protein that functions at multiple steps of higher plant nuclear pre-mRNA maturation. EMBO J. 19, 1638–49. https://doi.org/10.1093/emboj/19.7.1638

Li, W., Li, † Y, Kedersha, N., Anderson, P., Emara, M., Swiderek, K.M., Moreno, G.T., Brinton, M.A., 2002. Cell Proteins TIA-1 and TIAR Interact with the 3 Stem-Loop of the West Nile Virus Complementary Minus-Strand RNA and Facilitate Virus Replication Downloaded from. J. Virol. 76, 11989–12000. https://doi.org/10.1128/JVI.76.23.11989-12000.2002

Linero, F.N., Thomas, M.G., Boccaccio, G.L., Scolaro, L. a, 2011. Junin virus infection impairs stress-granule formation in Vero cells treated with arsenite via inhibition of eIF2α phosphorylation. J. Gen. Virol. 92, 2889–99. https://doi.org/10.1099/vir.0.033407-0

Liu, D., Shi, L., Han, C, Yu, J, Li, D, Zhang, Y., 2012. Validation of Reference Genes for Gene Expression Studies in Virus-Infected Nicotiana benthamiana Using Quantitative Real-Time PCR. Plos One 7(9). https://doi.org/10.1371/journal.pone.0046451.

Lloyd, R.E., 2012. How do viruses interact with stress-associated RNA granules? PLoS Pathog. 8, e1002741. https://doi.org/10.1371/journal.ppat.1002741

Lorkovic, Z.J., Wieczorek Kirk, D.A., Klahre, U., Hemmings-Mieszczak, M., Filipowicz, W., 2000. RBP45 and RBP47, two oligouridylate-specifi hnRNP-like proteins interacting with poly (A) RNA in nuclei of plant cells. https://doi.org/10.1017/s1355838200001163

Ma, X., Nicole, M.-C.C., Meteignier, L.-V.V., Hong, N., Wang, G., Moffett, P., 2015. Different roles for RNA silencing and RNA processing components in virus recovery and virus-induced gene silencing in plants. J. Exp. Bot. 66, 919–32. https://doi.org/10.1093/jxb/eru447

Mäkinen, K., Lõhmus, A., Pollari, M., 2017. Plant RNA Regulatory Network and RNA Granules in Virus Infection 8, 1–15. https://doi.org/10.3389/fpls.2017.02093

Mahboubi H, Koromilas AE, Stochaj U., 2016. AMP Kinase Activation Alters Oxidant-Induced Stress Granule Assembly by Modulating Cell Signaling and Microtubule Organization. Mol Pharmacol. 2016 Oct;90(4):460-8. doi: 10.1124/mol.116.105494. Epub 2016 Jul 18.

Montero, H., Trujillo-Alonso, V., 2011. Stress granules in the viral replication cycle. Viruses 3, 2328–38. https://doi.org/10.3390/v3112328.

Nelson, B.K., Cai, X., Nebenführ, A., 2007. A multicolored set of in vivo organelle markers for co-localization studies in Arabidopsis and other plants. Plant J. 51, 1126–1136. https://doi.org/10.1111/j.1365-313X.2007.03212.x.

Panas, M.D., Ivanov, P., Anderson, P., 2016. Mechanistic insights into mammalian stress granule dynamics. J. Cell Biol. 215, 313–323. https://doi.org/10.1083/JCB.201609081.

Price, M., 1993. Multipartite nature of potato virus X. J. Virol. 67, 596–600.

Price, M., 1992. Examination of potato virus X proteins synthesized in infected tobacco plants. J. Virol. 66, 5658–61.

Reineke, L.C., Lloyd, R.E., 2013. Diversion of stress granules and P-bodies during viral infection. Virology 436, 255–67. https://doi.org/10.1016/j.virol.2012.11.017

Sement, F.M., Ferrier, E., Zuber, H., Merret, R., Alioua, M., Deragon, J.-M., Bousquet-Antonelli, C., Lange, H., Gagliardi, D., 2013. Uridylation prevents 3' trimming of oligoadenylated mRNAs.

Nucleic Acids Res. 41, 7115–27. https://doi.org/10.1093/nar/gkt465

Sesma, A., Castresana, C., Castellano, M.M., 2017. Regulation of Translation by TOR, eIF4E and eIF2α in Plants: Current Knowledge, Challenges and Future Perspectives. Front. Plant Sci. 8, 644. https://doi.org/10.3389/fpls.2017.00644

Sonenberg, N., Shatkin, A.J., Ricciardi, R.P., Rubin, M., Goodman, R.M., 1978. Analysis of terminal structures of RNA from potato virus X. Nucleic Acids Res. 5, 2501–12.

Sorenson, R., Bailey-Serres, J., 2014. Selective mRNA sequestration by OLIGOURIDYLATE-BINDING PROTEIN 1 contributes to translational control during hypoxia in Arabidopsis. Proc. Natl. Acad. Sci. 111, 2373–2378. https://doi.org/10.1073/pnas.1314851111

Stols, A.L.H., Hill-van der Meulen, G.W., Toen, M.K.I., 1970. Electron microscopy of Nicotiana glutinosa leaf cells infected with potato virus X. Virology 40, 168–170. https://doi.org/10.1016/0042-6822(70)90389-2

Tilsner, J., Linnik, O., Wright, K.M., Bell, K., Roberts, A.G., Lacomme, C., Santa Cruz, S., Oparka, K.J., 2012. The TGB1 Movement Protein of Potato virus X Reorganizes Actin and Endomembranes into the X-Body, a Viral Replication Factory. Plant Physiol. 158, 1359–1370. https://doi.org/10.1104/pp.111.189605

Valiente-Echeverría, F., Melnychuk, L., Mouland, A.J., 2012. Viral modulation of stress granules. Virus Res. 169, 430–437. https://doi.org/10.1016/j.virusres.2012.06.004

Weber, C., Nover, L., Fauth, M., 2008. Plant stress granules and mRNA processing bodies are distinct from heat stress granules. Plant J. 56, 517–530. https://doi.org/10.1111/j.1365-313X.2008.03623.x

White, J.P., Cardenas, A.M., Marissen, W.E., Lloyd, R.E., 2007. Inhibition of Cytoplasmic mRNA Stress Granule Formation by a Viral Proteinase. Cell Host Microbe 2, 295–305. https://doi.org/10.1016/j.chom.2007.08.006

White, J.P., Lloyd, R.E., 2012. Regulation of stress granules in virus systems. Trends Microbiol.

20, 175–183. https://doi.org/10.1016/J.TIM.2012.02.001

Xu, J., Chua, N.-H., 2011. Processing bodies and plant development. Curr. Opin. Plant Biol. 14, 88–93. https://doi.org/10.1016/j.pbi.2010.10.003

Zappa F, Wilson C, Di Tullio G, Santoro M, Pucci P, Monti M, D'Amico D, Pisonero-Vaquero S, De Cegli R, Romano A, Saleem MA, Polishchuk E, Failli M, Giaquinto L, De Matteis MA. 2019. The TRAPP complex mediates secretion arrest induced by stress granule assembly. EMBO J. Aug 20:e101704. doi: 10.15252/embj.2019101704.

Figure Legends.

Figure 1. Effect of PVX infection at early phase on SG formation. A) SG marker GFP:AtUBP1b expressing cells were infected with PVX and then samples were taken at 7, 12, 18, 24 and 48 h (T) post inoculation to evaluate SG formation. Bar=30 µm. B) PVX infection progress was determined by RT-PCR. Upper gel corresponds to PVX CP specific primers. Bands are visible in lanes 4 and 5. Lower gel corresponds to control actin primers. Lanes: 1 to 5 correspond to T7, T12, T18, T24, and T48.

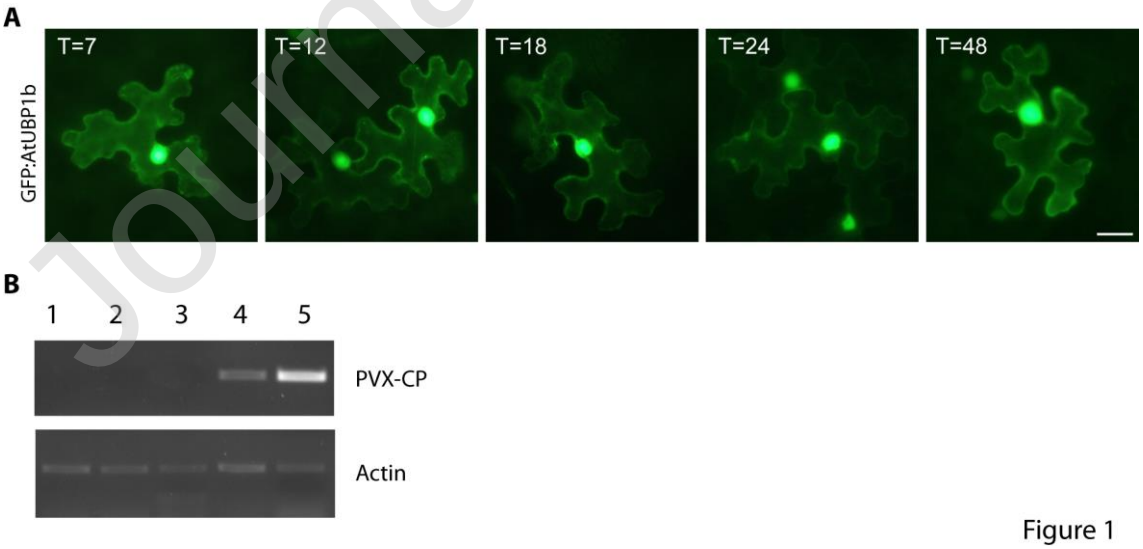

Figure 1

Figure 2. Effect of PVX infection at established late phase on SG formation. A) Upper row: i and ii are representative images of RFP:AtUBP1b expressed in the healthy cells, i: No hypoxia (t= 0 min) and ii: Hypoxia (t= 30 min) showing many SGs. Panels iii and iv are representative images of RFP:AtUBP1b expressed in the PVX infected cells, iii: No hypoxia (t= 0 min) and iv: Hypoxia (t= 30 min) with very few SGs. "N" indicates nucleus and "*" RFP:AtUBP1b cluster in panel iv. Bar=30 µm. Lower row: the relative motility of SGs determined from equivalent conditions described for i to iv, showing a color scale corresponding to each SG tracking obtained from the images of the videos (Supplemental materials). The white dots shown in panel iv indicates no movement of SGs. In contrast, colored tracking lines in panel ii indicate SGs movement. Bar=5 µm. B) Counting of SG/cell represented by the box plots chart. A comparative distribution of number of SG/cell corresponding to the conditions described in panels i to iv are shown from 2 representative experiments (see also supplemental tables). Hypoxia treated samples are indicated with shaded box. In addition, the SG/cell is charted from the co-expression of RFP:AtUBP1b and TGBp1:mCherry (hypoxia, t=30 min) experiments. * represents statistically significant areas p-value <0.05.

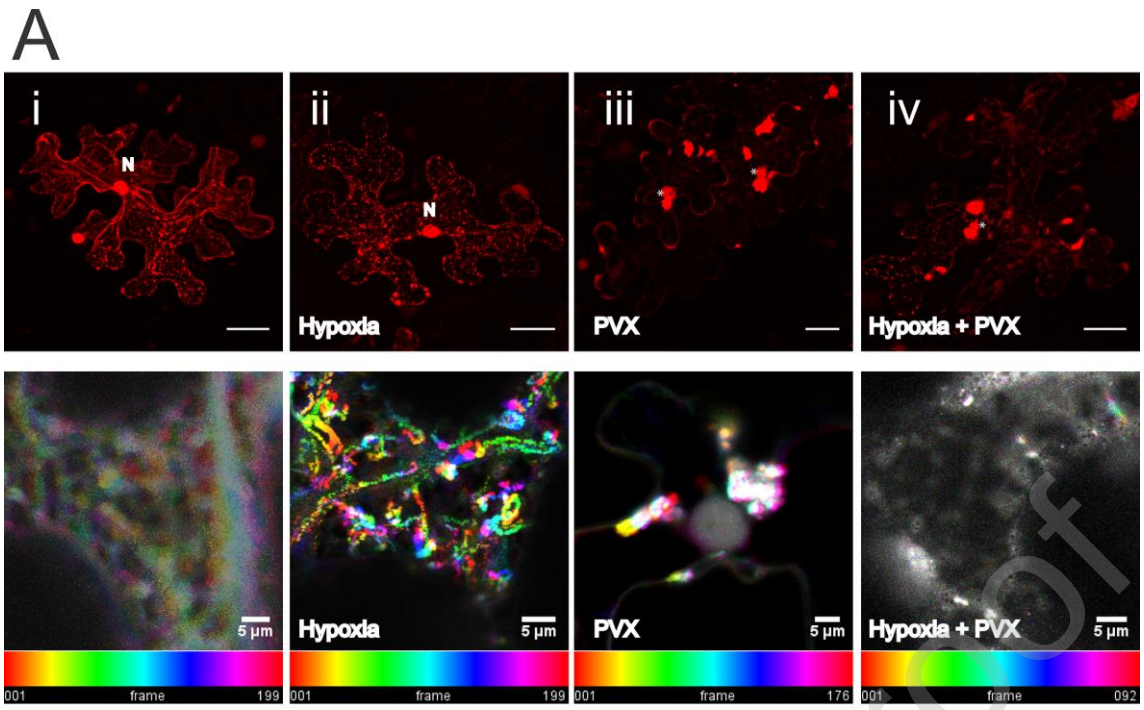

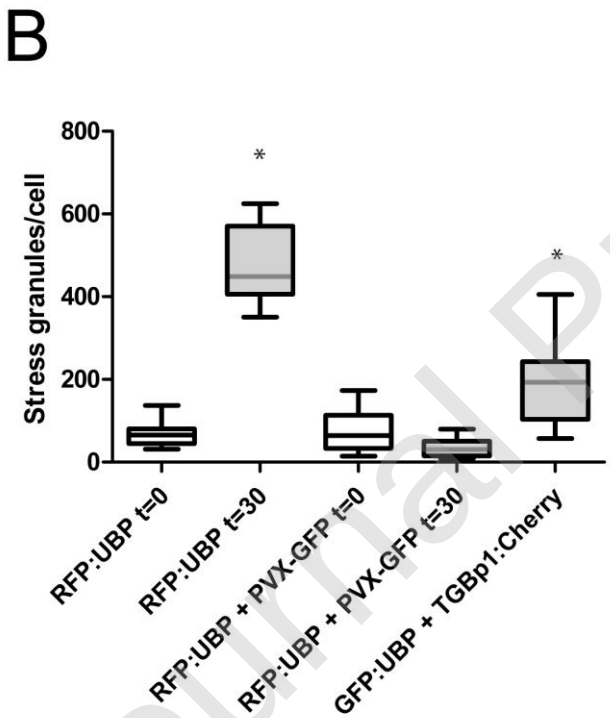

Figure 2

Figure 3. Virus induced cytoplasmic inclusion body relocates GFP:AtUBP1. A) A pseudo X-body revealed with TGBp1:mCherry and GFP:AtUBP1b in *N. benthamiana* healthy cell, under hypoxia stress. A cell contour was marked with white dot line in merge panel. Fibrous structures of TGBp1:mCherry seems to be entangling GFP:AtUBP1 and SGs-like granules. Bar=10 µm. B) Details of GFP:AtUBP1b cluster and some SGs-like granules in close proximity with X-body labelled by TGBp1:mCherry in PVX infected cell under hypoxia. Bar=5 µm.

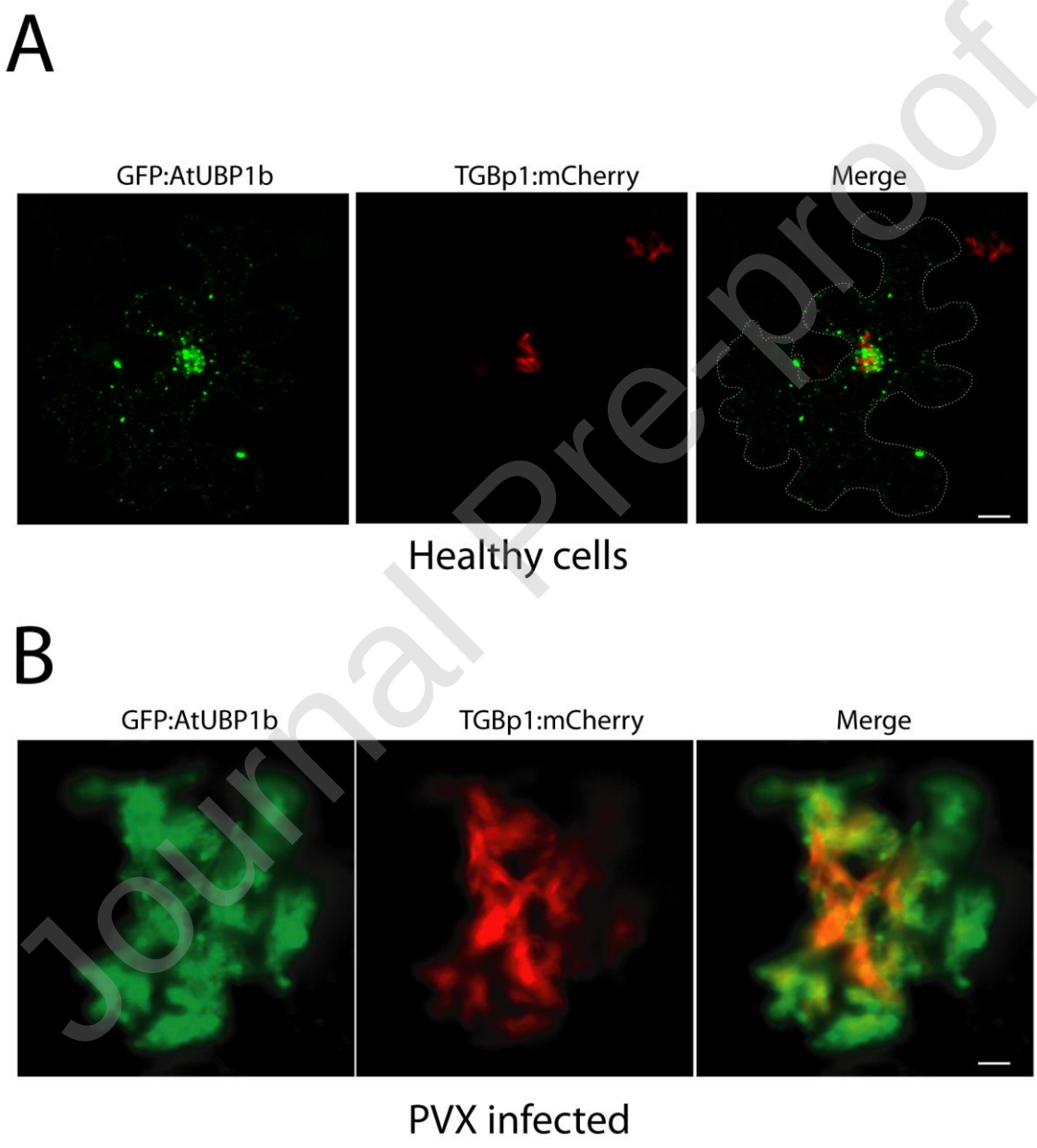

Figure 3

Figure 4. Effects of AtUBP1b during onset of PVX-GFP infection. A) Representative image of GFP foci in PVX-GFP infected *N. benthamiana* leaf expressing AtUBP1b, AtUBP1brrm, or mRFP at 5 dpi. B) Size distribution of PVX-GFP infection foci represented by box plot chart. ANOVA followed by Tukey comparison test were performed on values shown in the supplemental tables S4 and S5 (* p-value <0.05). C) Real-time RT-qPCR of PVX vRNAs. Relative expression levels of vRNAs CP in mRFP, AtUBP1b, or AtUBP1brrm expressing half leaves, using the actin gene as housekeeping. ANOVA followed by Tukey comparison test were performed (**p-value < 0.05). D) Protein extracts from the same leaves used for RT-qPCR analyses were evaluated by Western blot to estimate GFP expressed by PVX-GFP (upper blot). Red Ponceau staining (lower blot). Band intensities of GFP (GFP band int.) were obtained using Image J software by normalizing to the intensities of RFP control bands and Red Ponceau. Horizontal lines on the top of the blot indicate individual leaves from 6 different plants, while each lane corresponds to half of the leaf.

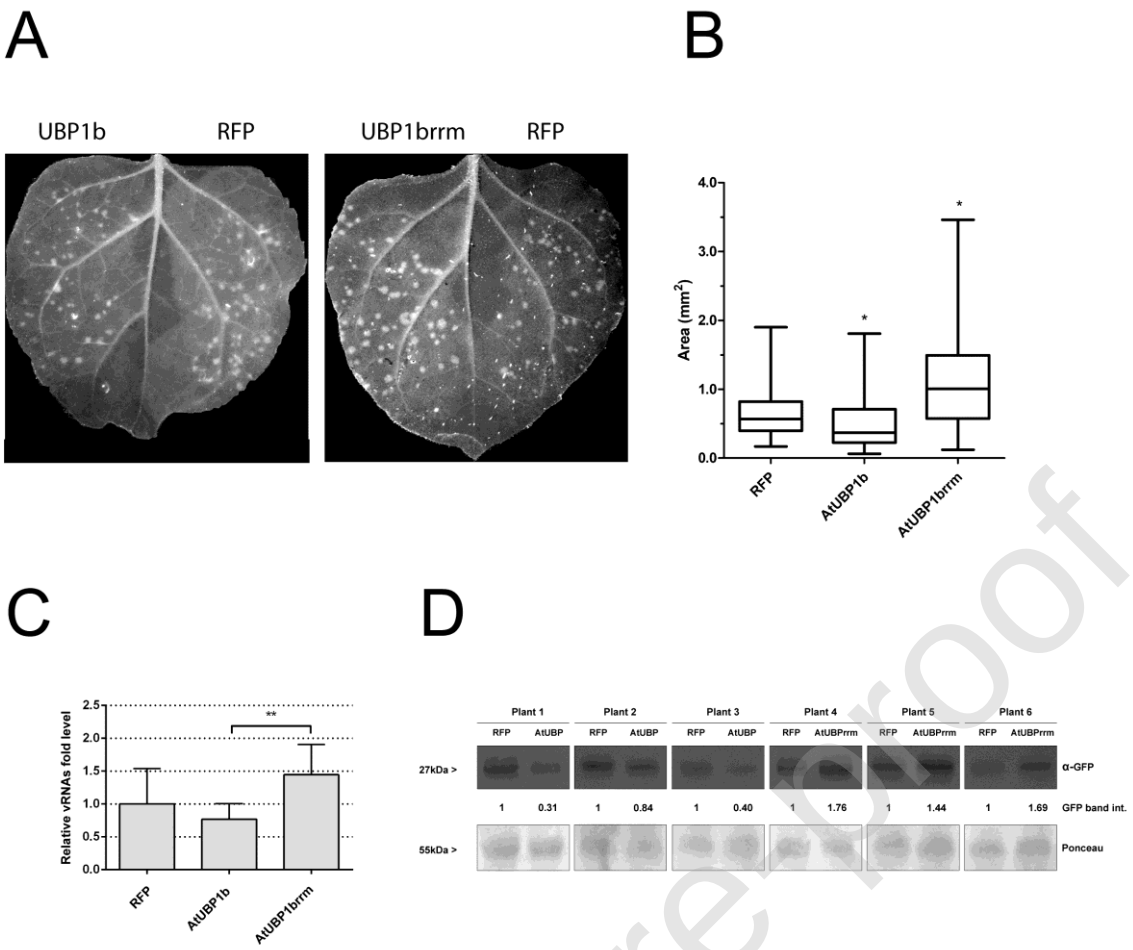

Figure 5. Effect of PVX infection on PB formation. A) Representative images of AtDCP1:RFP expressed in the healthy cells, i: No hypoxia (t= 0 min) and ii: Hypoxia (t= 30 min), and iii and iv are representative images of AtDCP1:RFP expressed in the PVX infected cells, iii: No hypoxia (t= 0 min) and iv: Hypoxia (t= 30 min) leaves at 5 dpi. Bar: 30 µm. B) The counting of PB number/cell representing the box plots chart. A comparative distribution of PB numbers is shown from 2 representative experiments (see also supplemental table S7). Hypoxia treated samples are indicated with shaded box. C) Boxes: size distribution of PVX-GFP infection foci in PVX-GFP infected *N. benthamiana* leaf expressing AtDCP1:RFP or mRFP at 5 dpi. ANOVA followed by Tukey comparison test were performed on values shown in the supplemental tables S4 and S6 (*p-value < 0.05).

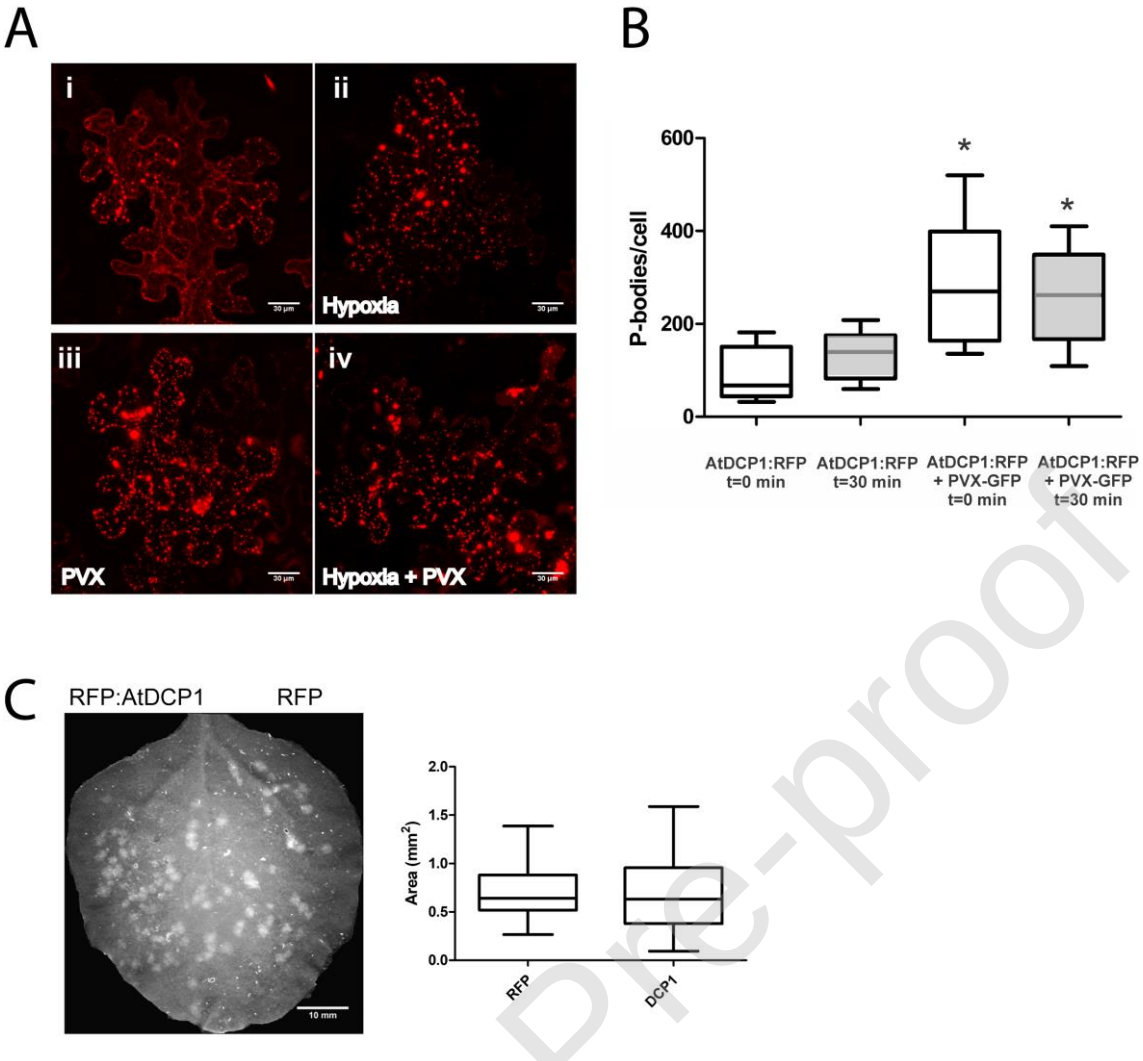

Figure 5